THE ASTROPHYSICAL JOURNAL, 349:126–140, 1990 January 20

ON THE FORMATION AND EXPANSION OF H II REGIONS[1]

JOSÉ FRANCO,[2,3] GUILLERMO TENORIO-TAGLE,[3] AND PETER BODENHEIMER[4]
Received 1989 March 27; accepted 1989 July 17

ABSTRACT

The evolution of H II regions in clouds with power-law density stratification r^{-w} and in isothermal self-gravitating gaseous disks is described analytically. For power-law profiles, there is a critical exponent, $w_{\rm crit}$, above which the ionization front cannot be "trapped" (i.e., the front is not slowed down by recombinations or new ionizations) and the cloud becomes fully ionized. This critical exponent can have different values during the formation and expansion phases. Its value in the formation phase depends on the internal grain opacity and assumed initial conditions (i.e., on the flux of the ionizing star and on the density and size of the cloud core). During the expansion phase, $w_{\rm crit} = 3/2$, and this value is independent of dust opacity and initial conditions. For clouds with $w < 3/2$, the ionized region expands as $t^{4/(7-2w)}$ and drives a shock front that accelerates and sweeps the ambient medium into a thin neutral shell. For $w = w_{\rm crit} = 3/2$, the shock wave cannot detach from the ionization front, and the two move together with a constant speed equal to about $2c_i$, where c_i is the sound speed in the ionized gas. For $w > 3/2$, the expansion follows the socalled "champagne phase" (i.e., the higher pressure, denser part of the cloud expands supersonically into the surrounding ionized medium). In such a case, two regimes, fast and slow, are apparent: between $3/2 < w \leq 3$ (the slow regime), the inner region drives a weak shock moving with almost constant velocity through the cloud, and for $w > 3$ (the fast regime), the shock becomes strong and accelerates with time.

In the case of isothermal self-gravitating disks, the dimensions of the initial H II region are direction dependent. The size along each azimuthal angle, θ, is described in terms of the Strömgren radius for the midplane density, R_0, and the disk scale height, H. For $y_0 = R_0 \sin(\theta)/H \leq 0.88$, the whole H II region is contained within the disk, and for $y_0 > 0.88$, a conical section of the disk becomes fully ionized. The critical azimuthal angle above which the H II region becomes unbounded is defined by $\theta_{\rm crit} = \sin^{-1}(0.88H/R_0)$. For $y_0 \simeq 1$ and in the absence of magnetic fields, the expansion produces a "variable" stage during which the ionization front is forced to recede from infinity and the H II region becomes ionization bounded. Such a trapping occurs during the early stages of the disk expansion and has a short duration.

The approximate analytical solutions are compared with detailed hydrodynamical numerical simulations of photoionized regions, and the agreement is shown to be better than 10%. Some applications for star-forming regions are outlined, and the approximate effects of dust opacity are also discussed.

Subject headings: hydrodynamics — nebulae: H II regions — nebulae: internal motions — shock waves

I. INTRODUCTION

Beginning with Strömgren (1939), the theory for the evolution of H II regions has been developed with a variety of analytical and numerical studies (see reviews by Kahn and Dyson 1965; Mathews and O'Dell 1969; Tenorio-Tagle 1982; Yorke 1986; and standard reference books by Osterbrock 1989 and Spitzer 1978). For a constant photon flux and uniform ambient densities, the evolution has well-defined formation and expansion phases. During the formation phase, soon after the radiation field of a hot star has been turned on, the energetic photons create a supersonic ionization front (termed weak R-type) that moves through the gas, leaving it hot and ionized but almost undisturbed. The speed of this front is reduced continuously by the geometrical dilution of the radiation field and by recombinations in the ionized volume until it approaches a value of about twice the speed of sound in the ionized gas. At such a time, which marks the end of the formation phase, the dimensions of the ionized region reach the "initial" Strömgren radius. The large pressure gradient across the ionization front then derives the expansion of the ionized gas. This expansion is supersonic with respect to the ambient neutral material and creates a shock wave that sweeps, accelerates, and compresses the surrounding medium. The ionization front, on the other hand, evolves into a subsonic disturbance (i.e., changes from weak R-type into a D-type front) and sits behind the shock front during the rest of the evolution, while, gradually, neutral gas accumulates in the interphase between the two fronts.

Departures from the evolution described above result from changes in the boundary and initial conditions of the problem. The most natural alternative, given that massive stars seem to form in molecular clouds, is to relax the assumption of a constant ambient density. If either the ionization or the shock front encounters a strong negative density gradient (say, the edge of the cloud) and overruns it, then the H II region will enter into its "champagne" phase. This is a supersonic expansion of the ionized gas promoted by the negative density gradient. Numerical models of H II region evolution under such circumstances have provided an explanation of the apparent morphology of ionized nebulae located near the edges of molecular clouds (see Tenorio-Tagle 1982). These models have also described the rate at which the ionized gas, previously molecular material, is expelled away from the molecular cloud, placing upper limits on the lifetime of star-forming clouds

[1] UCO/*Lick Observatory Bulletin* No. 1143.
[2] Instituto de Astronomía–UNAM, México.
[3] Max-Planck-Institut für Astrophysik, Federal Republic Germany.
[4] University of California Observatories/Lick Observatory, Board of Studies in Astronomy and Astrophysics, University of California, Santa Cruz.

(similar limits have been obtained with analytical approximations by Whitworth 1979). Also, given that the disrupted cloud matter preserves its momentum after recombination, the "champagne" phase has also been suggested as one of the sources for the velocity dispersion of the H I constituent of the galaxy (Larson 1987). The first models of this kind assumed abrupt discontinuities between constant density molecular and intercloud phases. Molecular clouds, however, have complex morphologies and density distributions, and they could be envisioned as hierarchical structures composed of a variety of high-density condensations (see Scalo 1985). These high-density condensations, or cloud fragments, seem to be the actual sites of star formation (see review by Shu, Adams, and Lizano 1987), and the initial shape and early evolution of the resulting H II regions depend on the corresponding fragment density distributions.

Theoretical studies on the initial stages of star formation indicate that either rotating or magnetic protostellar fragments should evolve into flattened disk-like structures (e.g., Bodenheimer and Black 1978; Cassen, Shu, and Terebey 1985), whereas the nonrotating and nonmagnetic ones can be regarded as spherically symmetric with power-law density distributions (e.g., Larson 1974). In particular, isothermal spheres in hydrostatic equilibrium have a density distribution proportional to r^{-2}, and the distribution evolves toward $r^{-3/2}$ during the free-fall collapse.

Recent observational studies on dark clouds and young stellar objects are beginning to uncover the structure of star-forming regions, and some of these results seem to provide support for the expected general features in the density distributions. Radio observations of cloud fragments and isolated dark clouds indicate internal density distributions proportional to r^{-w}, with w ranging from 1 to 3 and having an average at about $w \sim 2$ (Arquilla and Goldsmith 1985; see also Myers 1985). Visual extinction studies in nearby northern and southern clouds also indicate similar density gradients (Cernicharo, Bachiller, and Duvert 1985; Gregorio Hetem, Sanzovo, and Lepine 1988). Radio observations with high angular resolution in star-forming regions, on the other hand, have revealed the presence of elongated dense structures around recently formed stars, suggesting the possible existence of disk-like protostellar fragments (e.g., Torrelles *et al.* 1983). Similarly, optical and infrared data of several young stellar objects display a variety of features which can be ascribed to dusty circumstellar disks (e.g., Harvey 1985; Kenyon and Hartmann 1987).

Thus, one can explore the whole range of expected and observed density distributions in star-forming regions by considering (i) spherical clouds with power-law density profiles, $n(r) \sim r^{-w}$, and (ii) self-gravitating gaseous disks. In §§ II and III, we derive analytical solutions for the formation and expansion of H II regions for these two types of density stratifications. Magnetic fields are not considered here, but the approximate corrections resulting from the opacity of dust grains are discussed in an appendix. In all cases, the ambient gas is assumed to be originally at rest, and the source of ionization is thought to remain constant after it has been switched on. Thus, the details of gas accretion and luminosity changes during the stellar pre–main-sequence stages are ignored (a discussion of the evolution of ionization fronts during the late phases of protostellar accretion can be found in Yorke 1986, and numerical models for the expansion of compact H II regions in dusty clouds during the free-fall collapse are described by Cochran and Ostriker 1977 and Igumentshchev and Shustov 1989). A comparison of the analytical solutions with detailed hydrodynamical simulations of photoionized regions is given in § IV. A brief discussion of possible applications of these results and some forthcoming work is outlined in § V.

II. H II REGIONS IN POWER-LAW DENSITY DISTRIBUTIONS

Let us assume a spherical cloud with a molecular density distribution that includes a central core, with radius r_c and constant density n_c, and an envelope with a power-law density stratification

$$n_{\rm H_2}(r) = \begin{cases} n_c\,, & \text{for} \quad r \le r_c\,, \\ n_c(r/r_c)^{-w}\,, & \text{for} \quad r \ge r_c\,. \end{cases} \tag{1}$$

Here we are interested in positive values of the exponent (i.e., decreasing density gradients), but most results are quite general and are also valid for $w < 0$.

A star located at the cloud center and producing F_* ionizing photons per unit time will create a spherical H II region. The gas in this H II region is assumed to be fully ionized, and, hence, the ion density there is twice the molecular density, $n_i = 2n_{\rm H_2}$. One can define a reference dimension R_S (the Strömgren radius generated by such a star in a medium of constant density equal to n_c) to make some initial diagnostics,

$$R_S = \left[\frac{3F_*}{4\pi(2n_c)^2\alpha_B}\right]^{1/3} \simeq 0.2F_{48}^{1/3}n_3^{-2/3}\alpha_0^{1/3}\ \text{pc}\,, \tag{2}$$

where α_B is the hydrogen recombination coefficient to all levels above the ground level $\alpha_0 = \alpha_B/2.6 \times 10^{-13}\ \text{cm}^3\ \text{s}^{-1}$, $F_{48} = F_*/10^{48}\ \text{s}^{-1}$, and $n_3 = n_c/10^3\ \text{cm}^{-3}$.

a) The Formation Phase

For $R_S \le r_c$, the H II region is contained within the core and the formation phase follows the well-known constant density evolution. In the small-core case, $r_c < R_S$, the initial ionization front reaches the core radius in a time scale (e.g., Spitzer 1978)

$$t_c \simeq 130\alpha_0^{-1}n_3^{-1}\ln\left[\frac{1}{1-(r_c/R_S)^3}\right]\ \text{yr}, \tag{3}$$

and with a speed

$$U_c \simeq 90\alpha_0 n_3 r_{17}\left[\left(\frac{R_S}{r_c}\right)^3 - 1\right]\ \text{km s}^{-1}\,, \tag{4}$$

where $r_{17} = r_c/10^{17}$ cm. Afterward, the ionization front enters the density gradient, and its speed evolves as

$$U_{\rm if} = \frac{U_c}{(R_S/r_c)^3 - 1}\,u(w)\,, \tag{5}$$

with

$$u(w) = \begin{cases} (r_c/r_i)^{2-w}[(R_S/r_c)^3 + 2w\beta - 3\beta(r_i/r_c)^{1/\beta}]\,, \\ \qquad\qquad\qquad \text{for} \quad w \ne 3/2\,, \\ (r_c/r_i)^{1/2}[(R_S/r_c)^3 - 1 - 3\ln(r_i/r_c)]\,, \\ \qquad\qquad\qquad \text{for} \quad w = 3/2\,, \end{cases} \tag{6}$$

where r_i is the location of the front and

$$\beta = (3 - 2w)^{-1}\,. \tag{7}$$

Equation (5) is valid up to the moment when U_{if} decreases down to a value equal to $\sim 2c_i$, where c_i is the sound speed in the ionized gas (i.e., Osterbrock 1989; Spitzer 1978). At this moment, which defines the end of the formation phase, the ionization front changes from weak R-type into D-type, and the ionized region reaches a radius R_w (i.e., the "initial" size of the H II region) and begins to expand, driving a shock into the surrounding gas.

The size of the initial H II region is derived, as usual, by equating the total number of ionizing photons emitted by the star per unit time to the total number of recombinations per unit time within the ionized volume. For $w \neq 3/2$, this initial radius can be written as

$$R_w = g(w) R_S , \tag{8}$$

with

$$g(w) = \left[\frac{3-2w}{3} + \frac{2w}{3}\left(\frac{r_c}{R_S}\right)^3\right]^{\beta}\left(\frac{R_S}{r_c}\right)^{2w\beta} , \tag{9}$$

and the solution for $w = 3/2$ is

$$R_{3/2} = r_c \exp\left\{\frac{1}{3}\left[\left(\frac{R_S}{r_c}\right)^3 - 1\right]\right\} . \tag{10}$$

Equations (6) and (9) define a critical exponent for the formation phase, w_f, above which the solution for R_w does not exist, or the H II region can be regarded as unbounded. That is, the initial ionized region has a finite size for w smaller than

$$w_f = \frac{3}{2}\left[1 - \left(\frac{r_c}{R_S}\right)^3\right]^{-1} , \tag{11}$$

and it grows to infinity, without reaching the condition $U_{if} \simeq 2c_i$, for larger values of the exponent. Thus, this critical exponent corresponds to the maximum density gradient that is able to "trap" the ionization front (i.e., recombinations and new ionizations in steeper gradients are not sufficient to slow down the ionization front, which remains indefinitely as a weak R-type front). Note that for $R_S/r_c > 2$, the critical value becomes $w_f \simeq 3/2$.

The concept of a critical exponent is not necessarily restricted to power-law stratifications and can also be applied to other types of density distributions, for instance, exponential, Gaussian, and sech^2 profiles. The latter is discussed in § III.

b) *The Expansion Phase for w ≤ 3/2*

After the formation phase has been completed in clouds with $w \leq w_f$, the pressure in the ionized region, which is several orders of magnitude larger than in the neutral unperturbed gas, drives a shock into the molecular ambient medium and the H II region begins its expansion phase. The transition between these phases cannot be treated analytically, and we simply assume that the shock evolution starts at the initial time, $t = 0$, when R_w is achieved. Also, given that the expansion is subsonic with respect to the ionized gas, the density structure inside the H II region can be regarded as uniform (i.e., the density gradients can be smoothed out in short time scales).

If the shock radius at time t is $R(t)$, then the total mass (neutral plus ionized) contained within that radius is

$$M_s(t) = \frac{4\pi\rho_c r_c^3}{3-w}\left\{\left[\frac{R(t)}{r_c}\right]^{3-w} - \frac{w}{3}\right\} \simeq \frac{4\pi}{3-w}\rho(R)R^3(t) , \tag{12}$$

where ρ_c is the mass density in the core, and $\rho(R)$ is the mass density at $R(t)$. Thus, the volume-averaged density internal to $R(t)$ is simply equal to

$$\langle\rho\rangle \simeq \frac{3}{3-w}\rho(R) . \tag{13}$$

Similarly, given the position of the ionization front, $R_i(t)$, the ionized mass grows as

$$M_i(t) = \frac{4\pi}{3}\rho_i(t)R_i^3(t) , \tag{14}$$

where $\rho_i(t)$ is the average ion mass density in the H II region. Neglecting the separation between the shock and ionization fronts (i.e., Spitzer 1978), $R_i(t) = R(t)$, the ratio of the mass enclosed within the shock front to the ionized mass is given by

$$\frac{M_s(t)}{M_i(t)} \simeq \left(\frac{3}{3-w}\right)\frac{\rho(R)}{\rho_i(t)} . \tag{15}$$

A simple analysis of the properties of this mass ratio indicates that the expansion is driven by the average ion density

$$\rho_i(t) \simeq \mu_i \frac{(9-6w)^{1/2}}{3-w}\left(\frac{3F_*}{4\pi\alpha_B}\right)^{1/2} R^{-3/2}(t) , \tag{16}$$

where μ_i is the mass per ion. With this definition, which has the correct behavior at $t = 0$ [i.e., $M_s(0) = M_i(0)$] and reduces to the usual definition for the constant density case, the mass ratio evolves as

$$\frac{M_s(t)}{M_i(t)} \simeq \left[\frac{R(t)}{R_w}\right]^{(3-2w)/2} . \tag{17}$$

This is, fortunately, a rather simple description of the evolution. Equation (17) indicates that (1) for $w < 3/2$, the interphase between the ionization front and the leading shock accumulates neutral gas and its mass grows with time to exceed even the mass of ionized gas, and (2) for $w = 3/2 = w_{crit}$, the two fronts move together without allowing the formation and growth of a neutral interphase. Note that the decreasing ratio predicted by the equation for $w > 3/2$ is physically meaningless and it indicates only that the ionization front overtakes the shock front (and proceeds to ionize the whole cloud). Thus, regardless of the value of the critical exponent for the formation phase, w_f, the expansion phase is characterized by a critical exponent with a well-defined value, $w_{crit} = 3/2$, which is independent of the initial conditions.

Given that w_f could be larger than w_{crit}, initially bounded H II regions in density gradients with $w > 3/2$ will become unbounded during their expansion phase. The ionization front will ionize the swept up matter and will break through the shock front, leading to a change from D-type back into a weak R-type ionization front. This effect has already been seen in numerical studies of photoionized regions expanding in steep density gradients (Welter 1980; Tenorio-Tagle *et al.* 1986; Noriega-Crespo *et al.* 1989). Furthermore, given that above $w = 1$ the dust opacity is a slowly varying function of distance (see Appendix), this critical exponent $w_{crit} = 3/2$ is not affected by dust absorption.

For uniform ion densities, the gas velocity immediately behind the ionization front is equal to about half of the ionization front speed, and, neglecting the pressure of the ambient medium and the velocity difference between the ionization and shock fronts [i.e., $R_i(t) = R(t)$], the expansion rate of the H II region is determined by the jump conditions of an isothermal shock front (e.g., Spitzer 1978):

$$V_s^2 = \dot{R}^2 = c_i^2 \frac{\rho_i(t)}{\rho(R)} \left[1 - \frac{\rho_i(t)}{4\rho(R)}\right]^{-1} . \tag{18}$$

A direct integration of this equation, as is usually done for the constant density case, can be performed only by dropping the term in brackets. From equations (15) and (17), the density ratio can be written as

$$\frac{\rho_i(t)}{\rho(R)} \simeq \left(\frac{3}{3-w}\right)\left[\frac{R_w}{R(t)}\right]^{(3-2w)/2} . \tag{19}$$

This expression shows that indeed the term in brackets in equation (18) can be neglected for $w \leq 0$, but is not negligible for positive values of w. Thus, one has to make a further approximation in order to get an adequate analytical solution for decreasing density gradients.

Using the volume-averaged density internal to the shock front, $\langle \rho \rangle / \rho(r) \simeq 3/(3-w)$ (eq. [13]), the term in brackets is approximated roughly by

$$\left[1 - \frac{\rho_i(t)}{4\rho(R)}\right]^{-1} \simeq \frac{12-4w}{9-4w} , \tag{20}$$

and the jump condition reduces to

$$\dot{R} \simeq c_i \left(\frac{12}{9-4w}\right)^{1/2} \left[\frac{R_w}{R(t)}\right]^{(3-2w)/4} , \tag{21}$$

which is now an easily integrable equation. This correction results in an overestimation of the expansion rate of about 10% in the constant density case, but it provides an adequate correction for positive values of w. In particular, for $w = 3/2$, the shock velocity becomes constant at about $\simeq 2c_i$, which is the minimum value of an R-type ionization front, and the bulk mass velocity immediately behind the front is about c_i.

The evolution for $w \leq 3/2$, then, can be approximated by

$$R(t) \simeq R_w \left[1 + \frac{7-2w}{4}\left(\frac{12}{9-4w}\right)^{1/2} \frac{c_i t}{R_w}\right]^{4/(7-2w)} . \tag{22}$$

A comparison between this simple analytical solution and the results of a detailed numerical treatment is given in § IV (see Fig. 2).

c) *The Expansion for* $w \geq 3/2$: *The "Champagne" Phase*

For $3/2 < w < w_f$, the ionization front eventually overtakes the shock, and soon the whole cloud becomes ionized. At that moment, the gas acquires the same temperature everywhere, and the pressure gradient simply follows the density gradient. All parts of the cloud are then set into motion, but the initial gas acceleration,

$$a(r) \simeq \frac{w c_i^2}{r_c}\left(\frac{r}{r_c}\right)^{-1} , \tag{23}$$

decreases with radial distance. The expanded core, now with a radius identical to the position of the overtaken shock, is the densest region and feels the strongest outward acceleration: the core expands faster than the outer parts and pushes the gas ahead of it. Thus, superposed on the general gas expansion, there is a wave driven by the fast-growing core (the wave location defines the size of the expanded core), and the cloud experiences the so-called "champagne" phase. This core expansion tends to accelerate with time, and two different regimes, separated by $w = 3$, are apparent: a "slow" regime with almost constant expansion velocities, and a "fast" regime with strongly accelerating shocks.

The slow regime corresponds to $3/2 < w < 3$. A simple approximation to compensate for the general cloud expansion, which gets better as time proceeds, is to asume a reference frame moving with a velocity equal to c_i. The core expansion rate in this frame is mildly supersonic, almost a sound wave, and its density is able to adjust to the average value given in equation (13), $\langle \rho_c \rangle \simeq 3\rho(r)/(3-w)$ (where r is the size of the expanded core). When the recombination time is shorter than the evolutionary time scale, the cooling is balanced efficiently by new recombinations and the evolution proceeds almost isothermally. In this case, the core grows approximately as

$$r(t) \simeq r_c + \left[1 + \left(\frac{3}{3-w}\right)^{1/2}\right] c_i t , \tag{24}$$

where for simplicity the initial radius of the denser part of the cloud has been set equal to r_c, the initial size of the core. This, however, is only strictly true for clouds with w larger than w_f, when no shock is overtaken. Similarly, the average density has a small radial dependence that has been dropped in the approximation, and the time evolution should have had an exponent slightly larger than unity (i.e., the perturbation speeds up with time and evolves into a mild shock).

For $w = 3$, the average core density is about $\langle \rho_c \rangle \simeq [1 + 3\ln(r/r_c)]\rho(r)$, and the integral

$$\int_1^x \{1 + [1 + 3\ln(x)]^{1/2}\}^{-1} dx$$

[with $x = r(t)/r_c$] can be fitted, for $x > 3$, by $0.35x^{0.91}$. Thus, for $t \geq r_c/c_i$, the isothermal growth is now approximated by

$$r(t) \simeq 3.2 r_c \left(\frac{c_i t}{r_c}\right)^{1.1} . \tag{25}$$

In this case, the exponent is clearly larger than unity, showing the explicit time dependence in shock location and velocity.

For $w > 3$, the fast regime, the shock acceleration increases with increasing values of the exponent. Also, the total cloud mass becomes finite and equal to $wM_c/(w-3)$, where M_c is the original core mass. The acceleration has important effects in the structure of the expanded core. In particular, given the increasing shock velocities, the gas velocities and compression factors behind the shock front are better represented by their values in strong adiabatic shocks. The resulting postshock temperatures and densities cannot relax to uniform values, and the structure of the shocked region becomes stratified in all the flow variables (i.e., increasing in temperature and velocity, and decreasing in density and pressure; see Zel'dovich and Raizer 1967). The recombination time also has a steep increase with radial distance. Recombinations are then quenched at large radii, and the external parts of the shocked region behave almost adiabatically for most of the evolution. In contrast, the dense innermost regions of the expanded core can expand isothermally for a relatively long period of time (also note that the fraction of the expanded core which can be treated isothermally decreases with increasing w). Thus, the thermodynamical behavior of the expansion varies with radial distance and the evolution cannot be treated in the usual manner.

A simple solution is obtained by assuming that the pressure at the shock front decreases as a power-law $p(r) \simeq 3(r/r_c)^{-\delta}p_c/(w-3)$, where $p_c = \rho_c c_i^2$ is the initial core pressure, and that the value of the gas velocity behind the front is equal to the one in adiabatic strong shocks. With these simplifications, the core expansion is approximated by

$$r(t) \simeq r_c\left[1 + \left(\frac{4}{w-3}\right)^{1/2}\left(\frac{\delta+2-w}{2}\right)\frac{c_i t}{r_c}\right]^{2/(\delta+2-w)}, \quad (26a)$$

and the only remaining problem, then, is to find out an appropriate expression for the exponent δ. Its range of values can be restricted with simple arguments. The time dependence in the case $w = 3$ (eq. [25]) would correspond to $\delta \simeq 2.8$, and this value is used as the lower bound. Similarly, a true adiabatic expansion of a fixed mass of gas requires $\delta = 5$. Given that the mass external to the core decreases with increasing w, this adiabatic value can be set as the upper bound for large w. Note, however, that $\delta = 5$ constrains the solutions to $w < 7$. Thus, one can assume that δ varies smoothly, from 2.8 to 5, in the range $3 < w \leq 7$. The simpler, linear variation is

$$\delta \simeq 0.55(w-3) + 2.8 . \quad (26b)$$

This linear expression has no real physical meaning, but, as shown in § IV*a*, it provides a sound approximation to the evolution.

III. H II REGIONS IN SELF-GRAVITATING GASEOUS DISKS

All stratifications likely to represent a gaseous disk decrease faster than any power law at large radii. Therefore, all these distributions have a critical point beyond which their density falloff is steeper than $r^{-3/2}$. If the ionization front reaches this critical point in the formation phase of the H II region, it will continue indefinitely as a weak R-type front and the region becomes unbounded, as in the case $w > w_f$. Otherwise, the critical point will be reached during the expansion phase, and the leading shock will be overtaken by the ionization front.

The disks have cylindrical symmetry, and the variables r, θ, and z are defined in Figure 1. The gas is assumed isothermal with a constant scale height, H, and the ionizing star is located at midplane. The density distribution along the z-axis in an isothermal self-gravitating disk is $n(z) = n_0 \,\mathrm{sech}^2\,(z/H)$, where n_0 is the density at midplane. The size of the corresponding initial ionized region is direction dependent and can be described as a function of the azimuthal angle θ. As stated above, there exists a critical point at which the region becomes unbounded. For spherically symmetric configurations, the critical point is defined by a certain value of the radius, but in this case it corresponds to a critical angle, $\theta_{\rm crit}$.

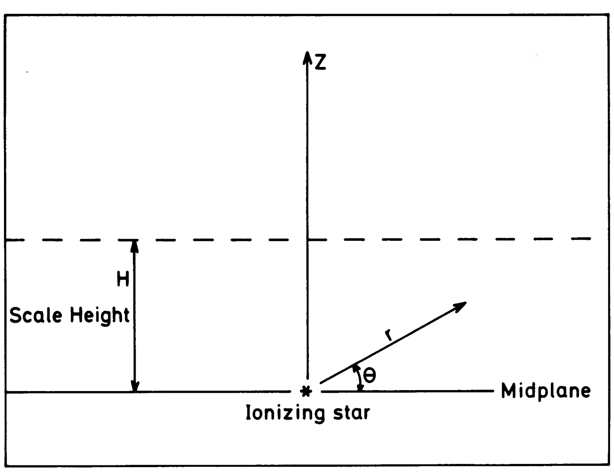

FIG. 1.—Schematic cross section of a gaseous disk with a star at midplane.

a) The Initial Shape of the H II *Region*

The treatment of this problem, which is performed by equating photoionizations and recombinations along each solid angle, requires the evaluation of the integral $\int_0^y y^2 \,\mathrm{sech}^4\,(y)dy$, where $y = r \sin(\theta)/H$. For small values of the variable y (i.e., y smaller than 1), the integration can be treated analytically and is simply approximated by $\tanh^3(y)/3$, but there are no general analytical solutions for arbitrary values of y. Keeping the functional form of the small-y solution, the integral can be approximated, to better than 5% over the whole range $0 \leq y \leq \infty$, by

$$\int_0^y y^2 \,\mathrm{sech}^4\,(y)dy \simeq 0.22 \tanh^3\left(\frac{y}{0.88}\right). \quad (27)$$

The particular functional form of the results presented below depends, of course, on this assumed fit. Nonetheless, the dimensions of the H II regions and the location of the critical point, $\theta_{\rm crit}$, do not depend on this choice (Franco, Tenorio-Tagle, and Bodenheimer 1989).

Here R_0 is defined as the Strömgren radius for the midplane density, and the additional parameter $y_0 = R_0 \sin(\theta)/H$ is useful in the description of the solution. The resulting size of the initial H II region as a function of the angle θ becomes

$$R_\theta \simeq R_0 h(\theta) , \quad (28)$$

with

$$h(\theta) = \left(\frac{0.44}{y_0}\right)\ln\left[\frac{1+(y_0/0.88)}{1-(y_0/0.88)}\right], \quad (29)$$

and the behavior for small values of y_0 (i.e., $y_0 \leq 0.3$) is

$$h(\theta) \simeq (1 + y_0^2/2) . \quad (30)$$

The equivalent average ion mass density along each line of sight weighted by the photoionization process (i.e., the ion density corresponding to a Strömgren radius of size R_θ), is given by

$$\langle\rho_i\rangle = \rho_0 h^{-3/2}(\theta) , \quad (31)$$

where ρ_0 is the mass density at midplane.

The critical point is $y_0 = 0.88$, and this corresponds to a critical angle

$$\theta_{\rm crit} = \sin^{-1}\left(0.88\,\frac{H}{R_0}\right), \quad (32)$$

which defines the conical section of the disk that is fully ionized. It is clear, then, that the initial H II region reaches the critical point when $R_0 > 0.88\,H$, and it becomes completely bounded within the disk when $R_0 \leq 0.88\,H$. Dust opacity reduces the dimensions of R_0 and R_θ (see Appendix), but the value of the critical point, $y_0 = 0.88$, remains unchanged.

b) The Expansion along the Symmetry Axis: "Variable-Size" H II *Regions*

The geometry of this problem is rather complex, and two-dimensional effects, such as lateral velocity components generated near the boundaries with the neutral gas, cannot be considered with a simple analytical scheme. Similarly, the transition from a bounded to an unbounded region (i.e., when the ionization front is able to break through the shock front) is also a two-dimensional problem. Thus, for simplicity, the analysis is focused on the expansion along the symmetry axis ($\theta = \pi/2$) of initially unbounded regions ($y_0 > 0.88$). Note that two-dimensional effects become important after a sound crossing time, $\tau_{2D} \simeq R_0/c_i$, and this restricts the discussion to the early stages of the expansion, $t < \tau_{2D}$. The symbols n_0, R_0, H, and y_0 are kept as the initial values (i.e., at $t = 0$) of the corresponding parameters.

The early stages of the expansion are controlled by the density gradient perpendicular to midplane, and the ionized gas flows only along the z-axis (see Bodenheimer *et al.* 1983). The initial acceleration,

$$a(z) \simeq \frac{2c_i^2}{H} \tanh\left(\frac{z}{H}\right), \tag{33}$$

increases with distance and becomes constant beyond the height $z \simeq 2\,H$. This acceleration stretches the disk and prevents the appearance of shock waves at early times. The gas velocities can, however, reach supersonic values. Note that the expansion changes the density gradient in a typical time scale of about $\tau_d \simeq (2\,H/c_i)$, and this change also modifies the gas acceleration. These variations are time dependent, and our approach is only valid before the time-dependent effects become important. Thus, the evolutionary time scales are restricted by the smaller value between τ_{2D} and τ_d (τ_{2D} is smaller for $y_0 < 2$, and $\tau_d < \tau_{2D}$ for $y_0 > 2$).

With these restrictions, the location of a gas particle along the axis evolves

$$z(t) \simeq z + \left(\frac{c_i^2 t^2}{H}\right) \tanh\left(\frac{z}{H}\right), \tag{34}$$

where z is the original height of the particle [in particular, note that the scale height grows as $H(t) \simeq H + 0.76c_i^2t^2/H$]. Mass is conserved and the column density from midplane to the location of any moving gas parcel, $N_{z(t)} = n_0 H \tanh(z/H)$, remains constant. The density distribution, $dN_{z(t)}/dz(t)$, also remains roughly similar to the original one, but now n_0 and H are replaced with $n_0(t)$ and $H(t)$. Defining $N_d = n_0 H$, the column density of the half-disk, the midplane density decreases as

$$n_0(t) \simeq N_d/H(t) \simeq n_0(1 + 0.76c_i^2t^2/H^2)^{-1} . \tag{35}$$

The equivalent Strömgren radius for this midplane density, $R_0(t)$, also increases as the expansion proceeds. The growth rates for $R_0(t)$ and $H(t)$ are different, however, and the dimensionless variable

$$y_0(t) = \frac{R_0(t)}{H(t)} = \frac{R_0}{H}\left[\frac{n_0(t)}{n_0}\right]^{1/3} , \tag{36}$$

is a decreasing function of time. Thus, there exists a time, τ_t, at which $y_0(t)$ drops below the critical value, 0.88, and the ionized region becomes trapped! At this time, the ionization front is forced to recede, and some gas recombines as a result of the expansion. This effect occurs when the midplane density reaches the value

$$n_0(\tau_t) \simeq (0.7) n_0\, y_0^{-3} , \tag{37}$$

and the corresponding trapping time is

$$\tau_t \simeq 1.2 y_0^{-1}\left[\left(\frac{y_0}{0.88}\right)^3 - 1\right]^{1/2} \tau_{2D} . \tag{38}$$

The constraint $\tau_t < \tau_{2D}$ indicates that the trapping can only occur for the cases $0.88 < y_0 \leq 1$. Also, given that the gas column density decreases after the rarefaction waves driven by the lateral expansion reach the symmetry axis, the trapping is shortlived, and after a time equal to τ_{2D}, the ionization front moves outward again. Thus, in the absence of magnetic fields, for cases with $y_0 \sim 1$, the H II region will have a "variable-size" stage shortly after it is born. Note that the recombining gas would be seen as a short-lived high-velocity neutral outflow. The main reason for the trapping is that the flow initially is primarily one-dimensional rather than spherical. The photon density always decreases faster than z^{-2} because of recombinations. The gas density distribution, which is initially steeper than any power law at large distances, becomes less steep during expansion. The increase in gas density at given heights can result in the trapping of a previously unbounded I-front.

A more general description for other disk-like density distributions, including the approximate effects of magnetic fields, is given in Franco, Tenorio-Tagle, and Bodenheimer (1989). Cases with magnetic field have longer lasting trappings and, consequently, can generate longer lasting high-velocity neutral outflows.

IV. COMPARISON WITH NUMERICAL SIMULATIONS

Radiative cooling from the metastable levels of heavy elements is very efficient (particularly from oxygen), so that the equilibrium temperature is fairly constant within the ionized region and is almost independent of the stellar effective temperature (e.g., Osterbrock 1989). Thus, the H II region can be regarded as isothermal, and for "cosmic" abundances, this equilibrium temperature is somewhat below 10^4 K. The resultant sound speed in the ionized gas is about $c_i \simeq 11.5$ km s^{-1}; this value will be used in the numerical simulations, which are performed with the procedure described by Tenorio-Tagle *et al.* (1986). The numerical grid resolution in all the models described in this section is 2.1×10^{15} cm, and the ambient gas is assumed atomic.

a) Power-Law Density Stratifications

Figure 2 shows a comparison between the analytical solutions (eqs. [22], [24], [25], and [26a]) and the detailed numerical simulations for various values of w. The stellar output is in all cases $F_* = 5 \times 10^{49}$ s^{-1}, and the core parameters are $n_c = 10^6$ cm^{-3} and $r_c = 2.1 \times 10^{16}$ cm. Figure 2*a* displays, as a function of time, the numerically obtained position of both ionization front and leading shock for $w = 1$. These in the analytical approach are assumed to be close together throughout the evolution (*solid line*). Figure 2*b* shows the critical case $w = 3/2$, where the fronts move together at a constant speed $\simeq 2c_i$. Figures 2*c* and 2*d* show a comparison for the cases with w equal to 3 and 5, respectively. The analytical solution for $w = 5$ was derived with $\delta = 3.9$ (eq. [26b]). The agreement in all cases is better than 10%. Similarly good agreement is obtained for $w = 1.7$ and 4.0.

Figures 3 and 4 display details of the numerical calculations, all performed with the same parameters indicated above, for $w = 1.4$, 1.5, 1.7, 3, and 5. Figure 3*a* ($w = 1.4$) shows the development and propagation of the leading shock, closely followed by the ionization front, as the H II region expands. The growing separation between the two fronts is not a result of accumulation but rather of slow radiative cooling of the gas at the postshock temperatures of several thousand degrees (e.g.,

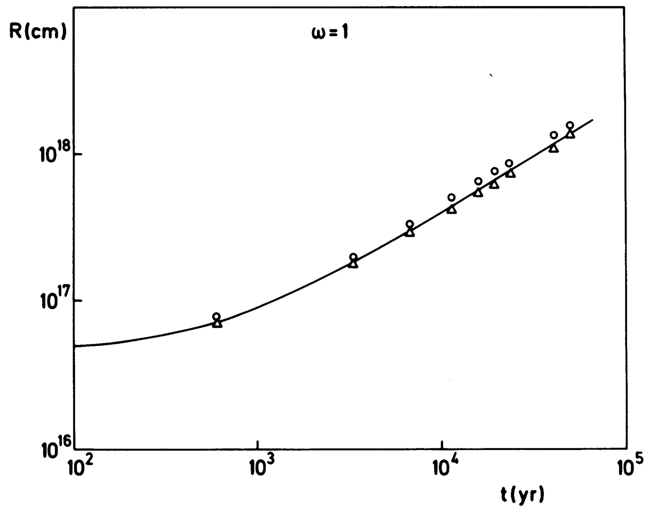

FIG. 2*a*

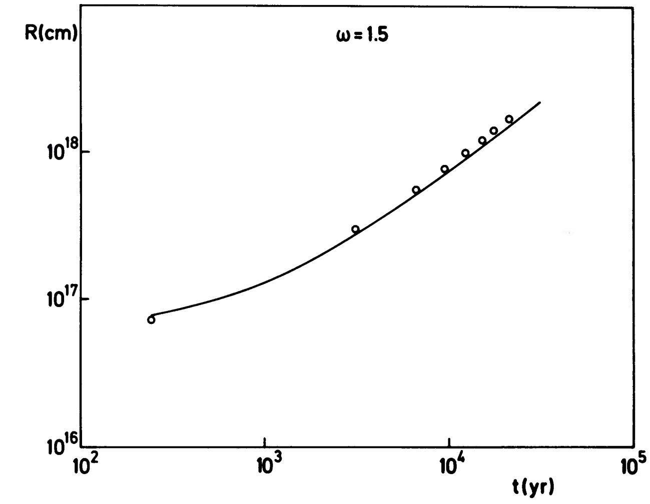

FIG. 2*b*

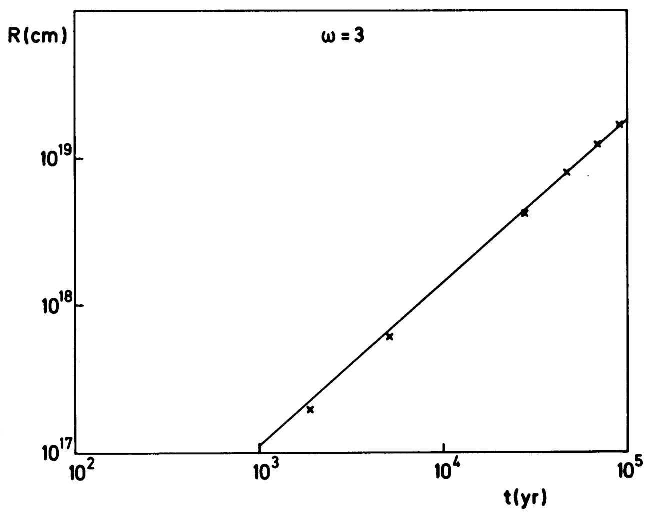

FIG. 2*c*

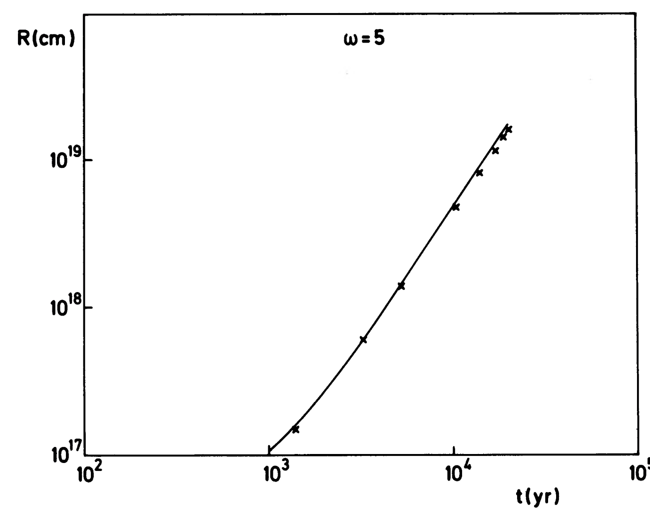

FIG. 2*d*

FIG. 2.—(*a*) Expansion of an H II region, with $w = 1$, $n_c = 10^6$ cm^{-3}, and $r_c = 2.1 \times 10^{16}$ cm, driven by a stellar photon output of $F_* = 5 \times 10^{49}$ s^{-1}. Solid line is the analytical approximation with $c_i = 11.5$ km s^{-1}. Numerical results for the ionization and shock fronts are marked with open triangles and open circles, respectively. (*b*)–(*d*) Same as (*a*), but for $w = 3/2$, 3, and 5, respectively.

Raymond, Cox, and Smith 1976). A shock under such conditions behaves quasi-adiabatically, while in the analytical approach it was assumed to be isothermal. Figure 3*b* shows the critical case $w = 3/2$. Comparing this with the preceding case, one can corroborate the predicted behavior of shock formation and propagation without accumulation of matter between the two fronts. Note that the density in the ionized volume in both cases acquires at all times fairly uniform values, in agreement with the assumptions made in the analytical approach. The numerical results for $w \leq 3/2$ are also in good agreement with the analytical prediction for the evolution of the ratio of total to ionized mass (eq. [17]). For $w = 1.7$, Figure 3*c*, the H II region has a formation phase (i.e., this case corresponds to $3/2 \leq w \leq w_f$), but the shock is overtaken by the ionization front almost immediately after the beginning of the expansion. At all times, the maximum value of the velocity is $\sim 2.5 c_i$, in agreement with the model predictions (eqs. [24]–[25]).

For large w values (Figs. 4*a*–4*b*), owing to the highly supersonic motions, the flow does not have sufficient time to relax to uniform values. In particular, as a result of the increase in shock velocity as a function of time, the density decreases and the gas velocity grows almost linearly inside the shocked region. For $w = 5$, at the last calculated time the velocity reaches a value of 350 km s^{-1}. The amount of matter with this

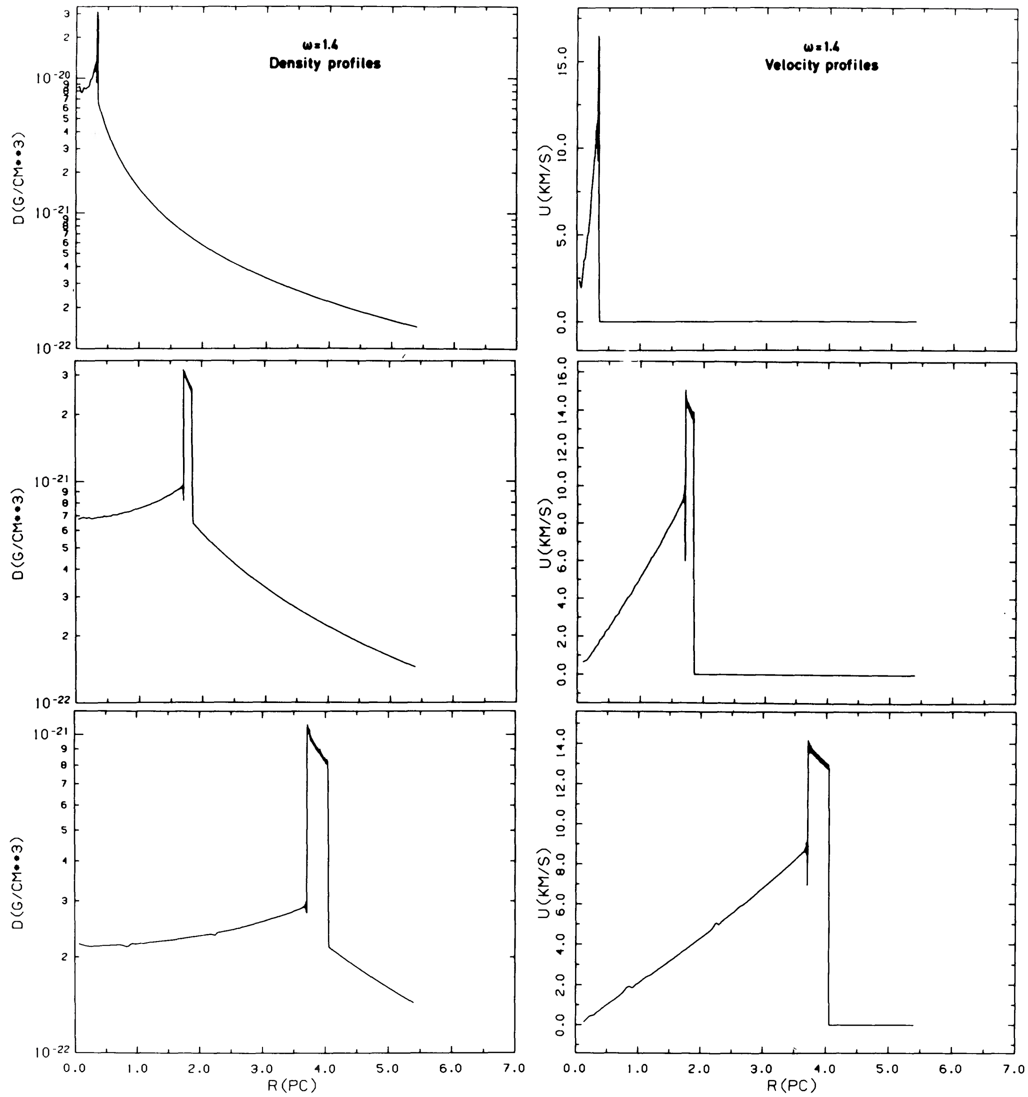

FIG. 3a

FIG. 3.—(a) Expansion of an H II region with $w = 1.4$ and the same parameters as in Fig. 2a. Density and velocity profiles are shown at $t = 1.39 \times 10^4$ yr, 9.1×10^4 yr, and 2.1×10^5 yr. (b) Same as (a), but for $w = 3/2$ at $t = 1.43 \times 10^4$ yr, 9.3×10^4 yr, and 1.7×10^5 yr. (c) Same as (a) for $w = 1.7$ at $t = 1.23 \times 10^4$ yr, 6.1×10^4 yr, and 1.72×10^5 yr.

high velocity is not very large. However, note that in both cases, the whole ionized cloud has attained supersonic speeds within the calculated evolutionary times.

b) Self-gravitating Disks

The numerical calculations for the hydrodynamics of photoionized regions in a stratified, self-gravitating disk were performed under the assumption of slab symmetry. The radiative transport was solved under the assumption of spherical symmetry. The initial midplane density was 10^3 cm^{-3}, and the ionizing flux was 3×10^{43} photons s^{-1}. The resulting reference radius was $R_0 = 2.87 \times 10^{16}$ cm. The scale height H was varied from 10^{16} cm to 5×10^{16} cm; these runs corroborate the limit for initially unbounded H II regions (when $R_0 \geq 0.88\,H$). Figure 5 shows details of the flow produced in an initially unbounded case with $H = 3 \times 10^{16}$ cm. At first, the whole disk becomes fully ionized and begins to expand in an almost homologous manner, preserving the shape of the initial density stratification. The gas velocity increases with height and becomes flat beyond $z = 2\,H$, as discussed in § IIb. The center frames show the moment when the midplane density has a value of about 7×10^2 cm^{-3}, at the time $t \simeq 520$ yr, and the ionization front becomes trapped. These values for the trapping are in fair agreement with the analytical expectations, $n_0(\tau_t) \simeq 8 \times 10^2$ cm^{-3} and $\tau_t \simeq 500$ yr (eqs. [37] and [38]). At $t = 850$ yr (*lower frames*), two-dimensional effects should begin

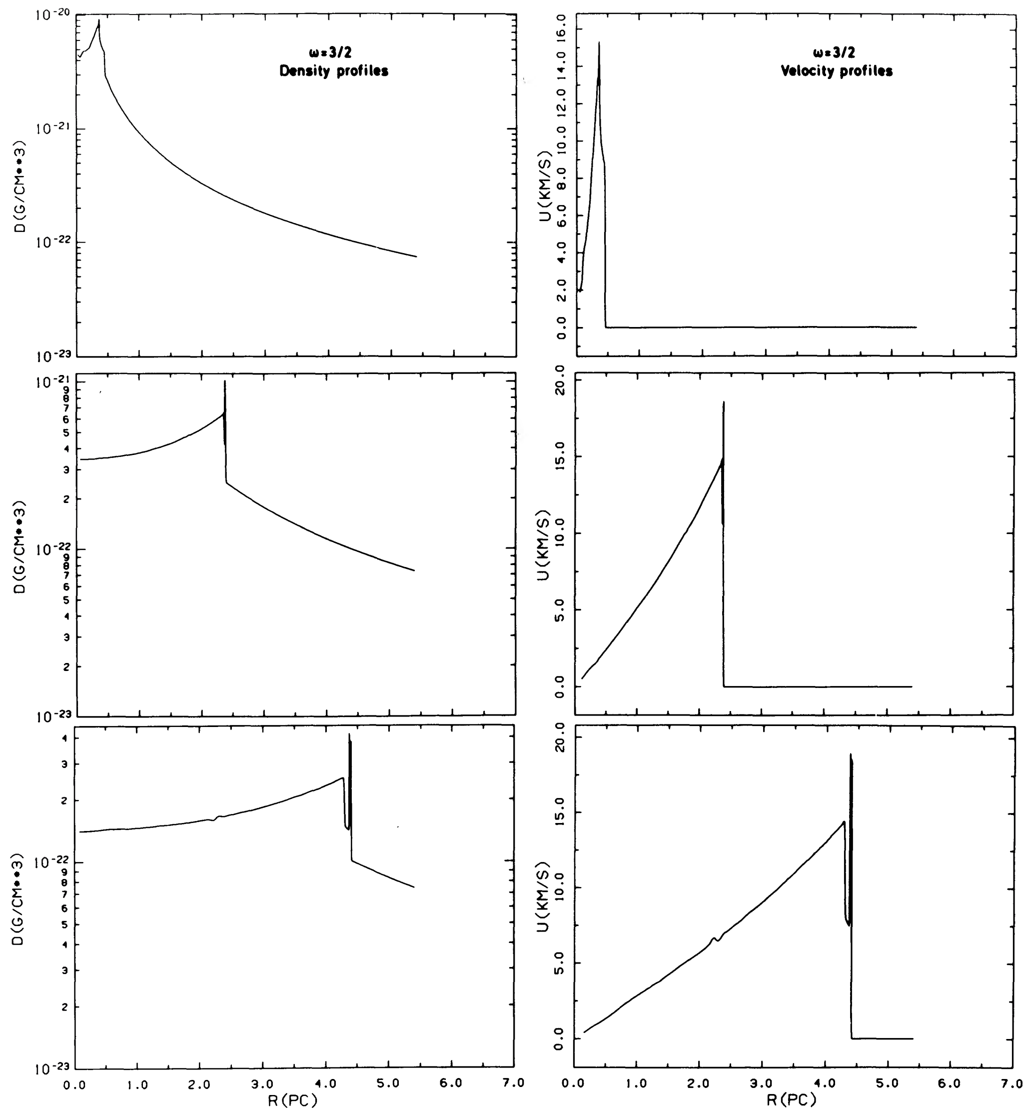

FIG. 3b

to reach the symmetry axis and should cause the front to move outward again. These details have been analyzed with a two-dimensional code by Franco, Tenorio-Tagle, and Bodenheimer (1989).

V. SUMMARY AND CONCLUSIONS

The results presented in this paper are meant to provide a physical insight into the variety of dynamical phenomena expected in H II regions, together with reliable tools to estimate their evolution under a wide range of conditions. For spherical clouds with a small constant-density core and a power-law density distribution, r^{-w}, outside the core, the results can be summarized as follows:

1. There is a critical exponent above which the cloud becomes completely ionized. Its value in the formation phase depends on the initial conditions, but it has a well-defined value, $w_{\rm crit} = 3/2$, during the expansion phase.

2. For $w < w_{\rm crit}$, the radius of the H II region grows as $t^{4/(7-2w)}$, while neutral mass accumulates in the interphase between the ionization and shock fronts. For $w = w_{\rm crit}$, the fronts move together without mass accumulation (i.e., the gas is ionized immediately after it is shocked), and the expansion velocity is constant at about $2c_i$.

3. Cases with $w > w_{\rm crit}$ lead to the champagne phase: once the cloud is fully ionized, the expansion becomes supersonic. The dense core expands faster than the rest of the ionized

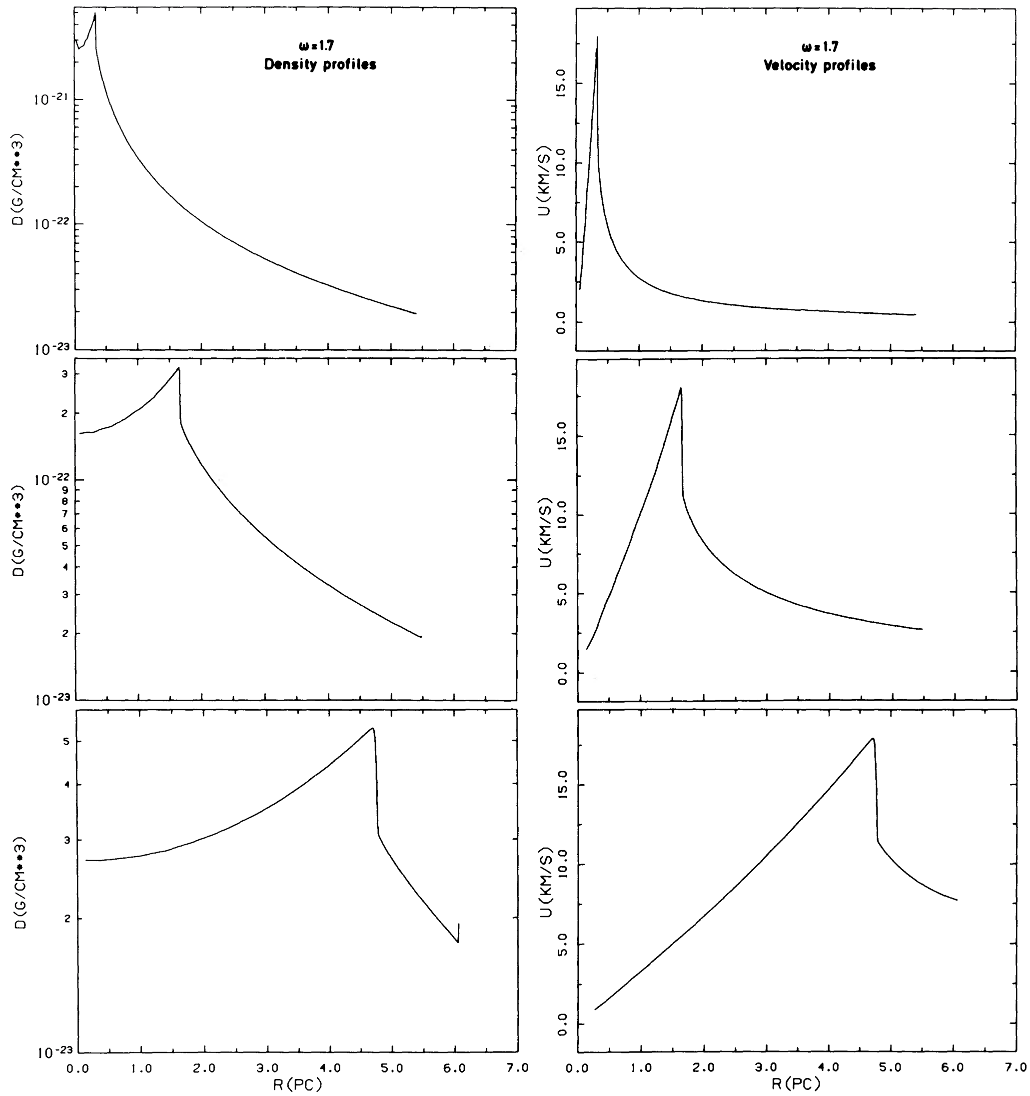

FIG. 3c

cloud, and a distinction between two well-defined regimes has been made. For $3/2 < w \leq 3$, the slow regime, the core expansion is mildly supersonic and has almost constant velocity. For $w > 3$, the the fast regime, the core expansion drives a strongly accelerating shock, and all the flow variables remain stratified during the evolution.

For self-gravitating disks without magnetic fields, the main features include a new "*variable-size*" stage:

1. The initial shape of the H II region has a critical point, $y_0 = 0.88$, which defines the azimuthal angle θ_{crit} beyond which the disk becomes completely ionized (this angle corresponds to the direction in which the density gradient becomes steeper than the critical value discussed for spherical clouds).

2. For initially unbounded H II regions ($y_0 > 0.88$), the gas flows along the z-direction during the early stages of the expansion. The one-dimensional analysis shows that the velocities increase with increasing height, up to $z \simeq 2\ H$, and the disk is stretched with time. For the particular case $y_0 \sim 1$, the H II region becomes bounded as a result of the expansion. This effect occurs in the very early stages of expansion and only lasts for a short period of time. Thus, regions with $y_0 \sim 1$ will have a highly variable size soon after their formation.

These results may also have a wide variety of possible applications. For instance, if the average density distribution of star-forming cloud fragments is truly steeper than $w = 3/2$, the parent fragments can be easily destroyed by the radiation field

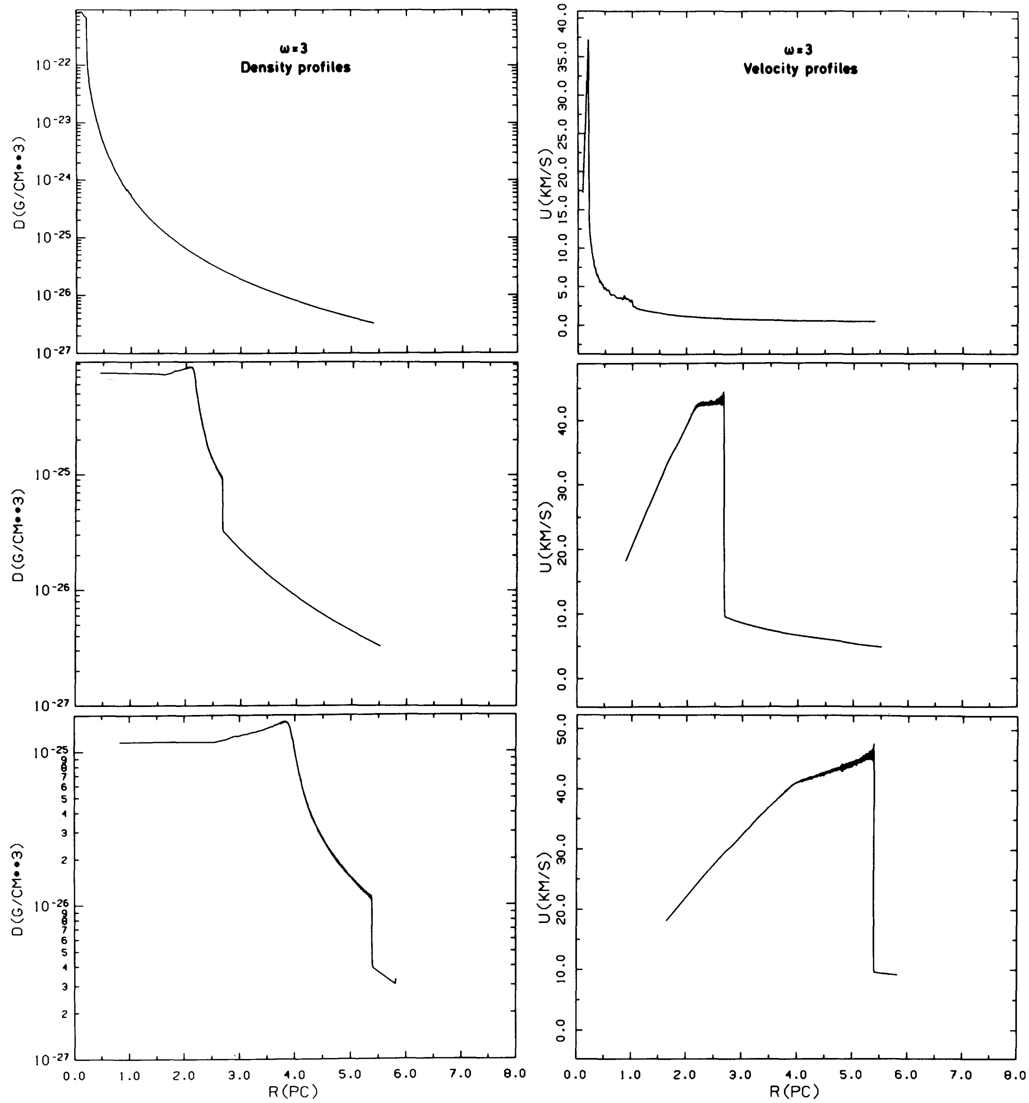

FIG. 4*a*

FIG. 4.—(*a*) Expansion of an H II region with $w = 3$ and the same parameters as in Fig. 2*a*. Density and velocity profiles are shown at $t = 5.12 \times 10^3$ yr, 4.9×10^4 yr, and 9.0×10^4 yr. (*b*) Same as (*a*) for $w = 5$ at $t = 5.29 \times 10^3$ yr, 1.7×10^4 yr, and 2×10^4 yr.

of recently formed massive stars. Moreover, all H II regions located at the cloud boundaries (i.e., the optical H II regions) are not ionization bounded in the outward direction, and there is a fraction of ionizing photons leaking out into the general interstellar medium (a similar situation may occur in planetary nebulae and even in active galactic nuclei). Such an asymmetry in the structure of optical nebulae indicates that the line ratios computed with ionization-bounded models may be misleading when compared with observed regions. In particular, ionization-bounded models require a harder UV spectrum (than do density-bounded models) to match the line ratios of different ionization species emitted by a density-bounded region. From the dynamical point of view, shocks driven by the expansion of the inner dense regions and running through the ionized gas may be quite common. Therefore, high-ionization species in young optical H II regions should have higher expansion velocities. Such a velocity stratification has already been reported for the Orion nebula (Wilson *et al.* 1959; Franco and Savage 1982): the absorption lines of high-ionization species such as C IV and Si IV are blueshifted some 25 km s^{-1} with respect to other nebular lines and some 40 km s^{-1} with respect to the exciting star. A previous interpretation (Franco and Savage 1982) ascribes the line shifts to the interaction of a stellar wind with high-density globules inside the nebula. The present results, however, show that similar shifts are also expected in density-bounded young regions with w between 2

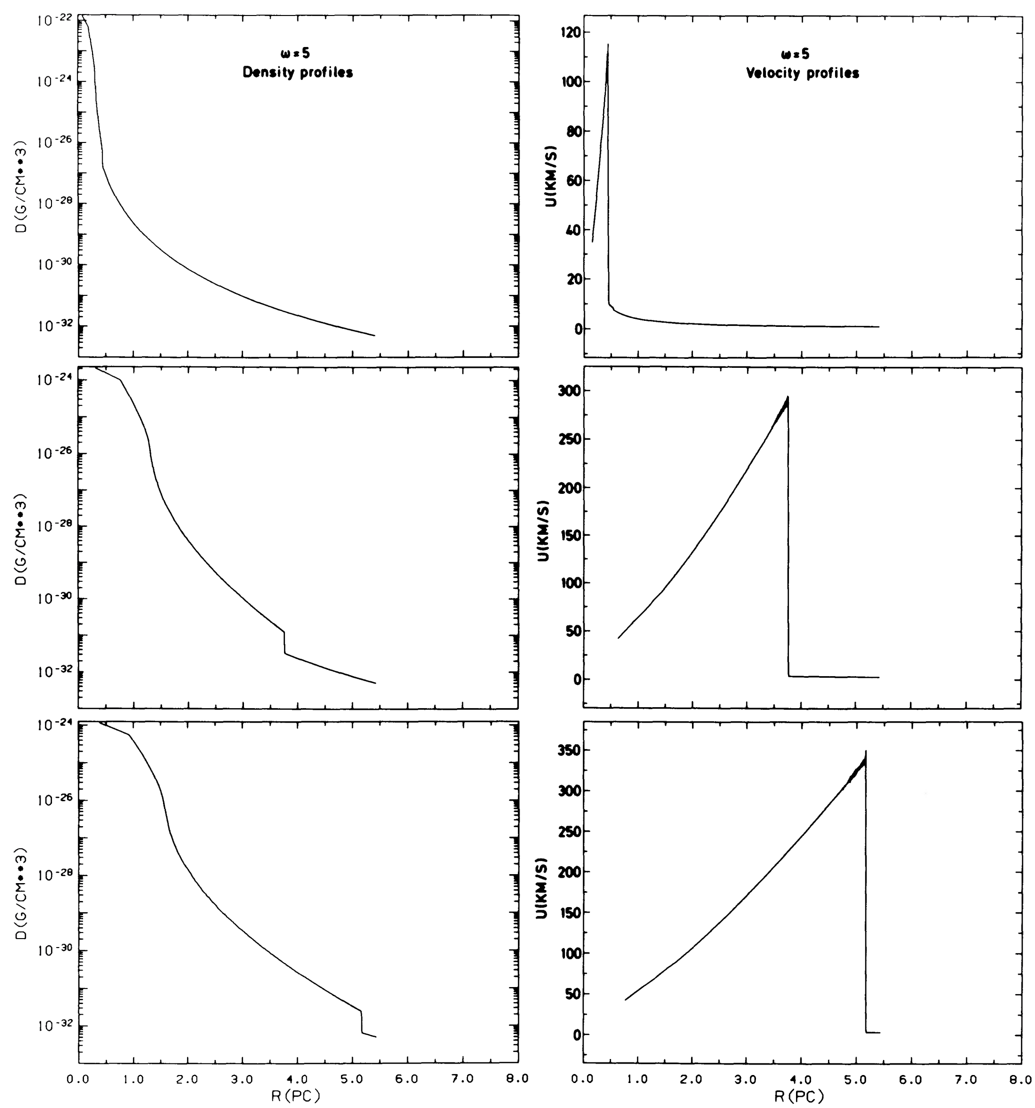

FIG. 4*b*

and 3 (eqs. [24] and [25]). Again, due to the possibility of strong internal shocks, line ratios derived from static photoionization models may not be reliable in the diagnostics of H II region complexes with intense star formation.

Another important point is the possibility of strongly accelerating shocks in regions with $w > 3$. These types of flows have been suggested as a source of cosmic-ray acceleration in supernova explosions when the shock emerges from the progenitor star (Zel'dovich and Raizer 1967), and the same effect may occur in some H II regions. The energies involved are obviously different, but the physical mechanism should be equally operative in the production of relativistic particles. This process may be linked with the γ-ray sources associated with star-forming regions (Montmerle 1985), and it certainly deserves further study.

In the case of self-gravitating disks, or in flat clouds, there are some similarities with the features described above. Again, the disks can be destroyed easily by massive stars, and the optical H II regions are not ionization bounded. The main difference between the disk and the spherical cloud cases is the possibility of a variable stage in the early disk evolution. This aspect was addressed for the particular case of a nonmagnetic $\mathrm{sech}^2(x)$ distribution. Nonetheless, it indicates that plane-stratified gas distributions undergoing an intense star-forming activity may present optical variability. Such a scenario could be important in understanding the light variations observed in

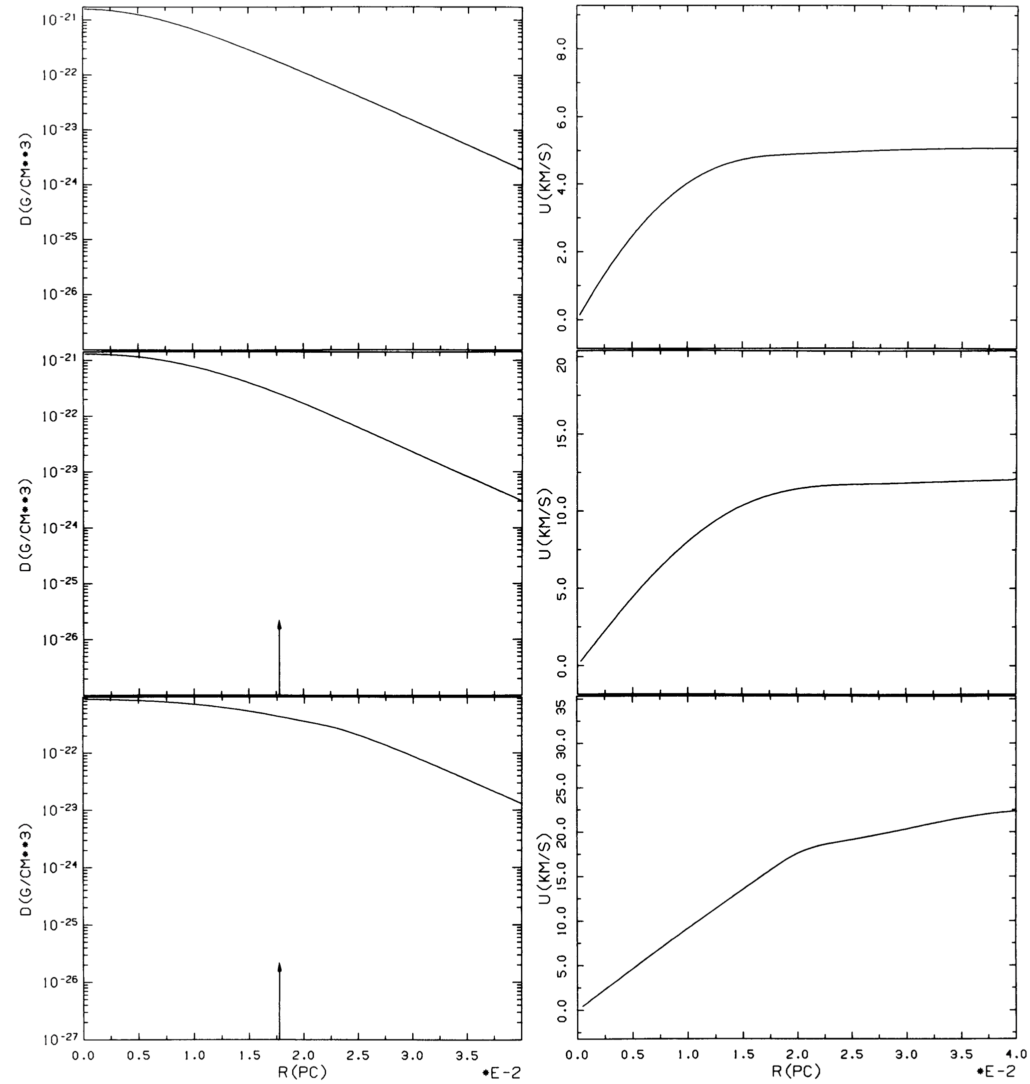

FIG. 5.—Expansion of an ionized disk. Density and velocity profiles along the symmetry axis are shown at (*top*) t = 185 yr, (*middle*) 520 yr, and (*bottom*) 850 yr. Arrow indicates the position of the trapped ionization front.

some active galactic nuclei. Similarly, the presence of a magnetic field can enhance the trapping stage and can lead to the existence of neutral flows (Franco, Tenorio-Tagle, and Bodenheimer 1989). Such flows should be connected with compact H II regions and should be detectable as high-velocity H I outflows. These features have some resemblance to observed properties of DR-21 (Russell 1987) and deserve a more detailed analysis. The case for the galactic gaseous disk was not considered in this study. However, these results indicate that OB associations should be pumping a substantial amount of ionizing photons into the galactic halo (and, perhaps, also to the intergalactic medium). The low densities involved in this case suggest that the high-latitude gas can remain ionized for a long period of time. Further studies with disk distributions are in progress and will be presented in a future paper.

We warmly thank R. Genzel, T. Hartquist, J. Mathis, and H. Yorke for very useful comments. In particular, Tom Hartquist provided many challenging questions during the initial stages of this study, and R. Genzel has been playing the devil's advocate. P. B. acknowledges the hospitality of the Max-Planck Institut für Astrophysik. He is supported in part by a special NASA astrophysics theory program through the joint Center for Star Formation Studies at NASA-Ames Research Center, University of California at Berkeley, and University of California at Santa Cruz. J. F. acknowledges partial financial support from CONACyT-México. G. T.-T. is supported by the Deutsche Forschungsgemeinschaft grant Mo 416.

APPENDIX

APPROXIMATE CORRECTIONS DUE TO DUST GRAINS

Dust grains absorb the stellar radiation and their opacity reduces the flux of ionizing photons available to the gas. The corresponding ionized region, then, is smaller than in the dust-free case. Dust scattering increases the probability for destruction of photons by gas and by other dust grains. Detailed numerical simulations for this process in constant-density H II regions show that dust scattering changes the details of the ionization structure, but that it has a rather minor effect (less than 10%) on the total number of recombinations (Mathis 1971). Hence, the net effect on the size of the ionized region is not important and can be neglected. For a constant dust-to-gas ratio, the dust optical depth for absorption is

$$\tau_d = \sigma_a N_g , \tag{A1}$$

where σ_a is the dust absorption cross section per gas particle, and N_g is the total gas column density. The dust cross section for absorption per gas particle depends, aside from the dust-to-gas ratio, on the average optical properties of interstellar grains. These, in turn, depend on their size distribution (e.g., Mathis, Rumpl, and Nordsieck 1977) and assumed grain composition (e.g. Draine and Lee 1984). Given that the efficiency of dust formation in nearby galaxies seems to be almost constant (e.g., Bouchet *et al.* 1985), a rough approximation to the dust absorption cross section per gas particle near the Lyman limit and as a function of the heavy element abundances, Z, can be written as (Franco and Cox 1986)

$$\sigma_a \simeq 2 \times 10^{-21}\left(\frac{Z}{Z_\odot}\right) \mathrm{cm}^2 , \tag{A2}$$

where $Z_\odot = 2 \times 10^{-2}$ is the "metallicity" in the solar neighborhood.

Assuming that the gas in the H II region is fully ionized, the total number of stellar ionizing photons available to the gas is reduced by dust opacity to, approximately,

$$F_d \simeq F_* e^{-\tau_d} , \tag{A3}$$

and the fraction of ionizing photons absorbed by the gas in the H II region is simply

$$f = e^{-\tau_d} , \tag{A4}$$

where τ_d is the optical depth at the boundary of the H II region. This approach, even though it neglects the detailed ionization structure of the region, provides reasonably good results. Figure 6 displays a comparison of equation (A4) with the detailed numerical simulations performed by Mathis (1971) and the analytical approximations derived by Petrosian, Silk, and Field (1972) for the constant-density case. As can be noticed from the figure, the departure from Mathis's more detailed results is always smaller than 20%. Moreover, given that the dimensions of the ionized region scale with $f^{1/3}$, the radii derived with this simple approach depart less than 10% from those derived with a more accurate method. Therefore, if the value of τ_d is known, one can approximate the initial size of H II regions in a dusty medium with the formulation described in the previous sections, but now replacing the original stellar output F_* with the reduced output F_d.

The value of τ_d at the boundary of the ionized region cannot be solved analytically for the general case of the density distributions discussed in the paper, and they have to be evaluated by iteration for each particular case. The required column densities and some of their properties are discussed below.

1. *Power-law density gradients.*—The column density at a distance r, larger than r_c, from the star is

$$N_g(r, w) = \begin{cases} n_c r_c(1 - w)^{-1}[(r/r_c)^{1-w} - w] , & \text{for} \quad w \neq 1 ; \\ n_c r_c[1 + \ln(r/r_c)] , & \text{for} \quad w = 1 . \end{cases} \tag{A5a}$$

For $w = 0$, the column density is simply proportional to the distance from the star. In this case, the value of τ_d and the reduction of

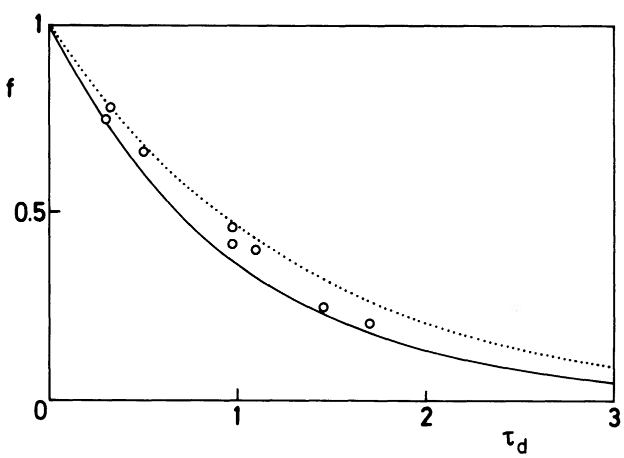

FIG. 6.—Fraction of ionizing photons absorbed by the gas plotted against the optical depth for true absorption in the ionized nebula. Solid line is eq. (A4), dotted line is the approximation of Petrosian, Silk, and Field (1972), the open circles are the numerical results of Mathis (1971).

the ionized region can be obtained with the approximations described by Petrosian, Silk, and Field (1972) or, alternatively, by solving the transcendental equation $R_d = R_S f^{1/3}$ (where R_d is the reduced radius of the H II region and R_S is the dust-free radius). Similarly, when the core optical depth is $\sigma_a n_c r_c \geq 3 \ln(R_S/r_c)$, the reduced H II region becomes trapped within the core, and, regardless of the value of w, its size is evaluated in the same manner as in the $w = 0$ case. The other cases (i.e., $w \neq 0$) do not have such a simple treatment, and one has to iterate the optical depth from equation (A5a) with equations (2), (8), and (9). For $w > 1$, however, the maximum column density amounts to $n_c r_c w/(w-1)$ and, as long as the reduced H II region is not trapped within the core, the differences in opacities between the dust-free and reduced regions are small. In these cases, the value of τ_d at the Strömgren radius for the dust-free case provides a good approximation to F_d. Also, given that the critical exponent for the formation phase depends on the ratio R_S/r_c and this ratio has now been reduced by dust absorption, the value of w_f is increased by a certain amount.

2. *Self-gravitating disks.*—The column density in this case becomes

$$N_g(r, \theta) = \frac{n_0 H}{\sin(\theta)} \tanh\left[\frac{r \sin(\theta)}{H}\right]. \quad \text{(A5b)}$$

The optical depth and its corresponding reduced stellar output, then, are now functions of the angle, $\tau_d(\theta)$, and $F_d(\theta)$, respectively. Defining $R_0(\theta) = R_0 e^{-\tau_d(\theta)/3}$ and the corresponding dimensionless variable $y_0(\theta) = R_0(\theta)\sin(\theta)/H$, the size of the reduced ionized region is given again by equation (26) if R_0 and y_0 are replaced by the newly defined variables. Note, however, that the value of the critical point, $y_0(\theta) = 0.88$, is a property of the solution and is not affected by these redefinitions. The maximum column density near $\theta = \pi/2$ is about $n_0 H$, and this value can be used to check if the H II region becomes completely contained within the disk. Such is the case when $\sigma_a n_0 H \geq \ln(1.15 R_0/H)$.

REFERENCES

Arquilla, R., and Goldsmith, P. F. 1985, *Ap. J.*, **297**, 436.
Bodenheimer, P., and Black, D. C. 1978, in *Protostars and Planets*, ed. T. Gehrels (Tucson: University of Arizona Press), p. 288.
Bodenheimer, P., Yorke, H. W., Tenorio-Tagle, G., and Beltrametti, M. 1983, in *IAU Symposium 101, Supernova Remnants and Their X-ray Emission*, ed. J. Danziger and P. Gorenstein (Dordrecht: Reidel), p. 399.
Bouchet, P., Lequeux, J., Maurice, E., Prévot, L., and Prévot-Burnichon, M. L. 1985, *Astr. Ap.*, **149**, 330.
Cassen, P., Shu, F. H., and Terebey, S. 1985, in *Protostars and Planets II*, ed. D. C. Black and M. S. Matthews (Tucson: University of Arizona Press), p. 448.
Cernicharo, J., Bachiller, R., and Duvert, G. 1985, *Astr. Ap.*, **149**, 273.
Cochran, W. D., and Ostriker, J. P. 1977, *Ap. J.*, **211**, 392.
Draine, B. T., and Lee, H. M. 1984, *Ap. J.*, **285**, 89.
Franco, J., and Cox, D. P. 1986, *Pub. A.S.P.*, **98**, 1076.
Franco, J., and Savage, B. D. 1982, *Ap. J.*, **255**, 541.
Franco, J., Tenorio-Tagle, G., and Bodenheimer, P. 1989, *Rev. Mexicana Astr. Af.*, in press.
Gregorio Hetem, J. C., Sanzovo, G. C., and Lepine, J. R. D. 1988, *Astr. Ap. Suppl.*, **76**, 347.
Harvey, P. M. 1985, in *Protostars and Planets II*, ed. D. C. Black and M. S. Matthews (Tucson: University of Arizona Press), p. 484.
Igumentshchev, I., and Shustov, B. 1989, *Soviet Astr.*, in press.
Kahn, F. D., and Dyson, J. E. 1965, *Ann. Rev. Astr. Ap.*, **3**, 47.
Kenyon, S. J., and Hartmann, L. 1987, *Ap. J.*, **323**, 714.
Larson, R. B. 1974, *Fund. Cosmic Phys.*, **1**, 1.
———. 1987, in *Starbursts and Galaxy Evolution*, ed. T. X. Thuan, T. Montmerle, and J. Tran Than Van (Gif Sur Yvette: Frontiere), p. 467.
Mathews, W. G., and O'Dell, C. R. 1969, *Ann. Rev. Astr. Ap.*, **7**, 67.
Mathis, J. S. 1971, *Ap. J.*, **167**, 261.
Mathis, J. S., Rumpl, W., and Nordsieck, K. H. 1977, *Ap. J.*, **217**, 425.
Montmerle, T. 1985, *19th Internat. Cosmic Ray Conf.* (La Jolla), **1**, 209.
Myers, P. C. 1985, in *Protostars and Planets II*, ed. D. C. Black and M. S. Matthews (Tucson: University of Arizona Press), p. 81.
Noriega-Crespo, A., Bodenheimer, P., Lin, D. N. C., and Tenorio-Tagle, G. 1989, *M.N.R.A.S.*, **237**, 461.
Osterbrock, D. E. 1989, *Astrophysics of Gaseous Nebulae and Active Galactic Nuclei* (Mill Valley: University Science Books).
Petrosian, V., Silk, J., and Field, G. B. 1972, *Ap. J. (Letters)*, **177**, L69.
Raymond, J. C., Cox, D. P., and Smith, B. W. 1976, *Ap. J.*, **204**, 290.
Russell, A. P. G. 1987, Ph.D. thesis, University of Cambridge.
Scalo, J. M. 1985, in *Protostars and Planets II*, ed. D. C. Black and M. S. Matthews (Tucson: University of Arizona Press), p. 201.
Shu, F. H., Adams, F. C., and Lizano, S. 1987, *Ann. Rev. Astr. Ap.*, **25**, 23.
Spitzer, L. 1978, *Physical Processes in the Interstellar Medium* (New York: Wiley).
Strömgren, B. 1939, *Ap. J.*, **89**, 526.
Tenorio-Tagle, G. 1982, in *Regions of Recent Star Formation*, ed. R. S. Roger and P. E. Dewdney (Dordrecht: Reidel), p. 1.
Tenorio-Tagle, G., Bodenheimer, P., Lin, D. N. C., and Noriega-Crespo, A. 1986, *M.N.R.A.S.*, **221**, 635.
Torrelles, J. M., Rodriguez, L. F., Cantó, J., Carral, P., Marcaide, J., Moran, J. M., and Ho, P. T. P. 1983, *Ap. J.*, **274**, 214.
Welter, G. L. 1980, *Ap. J.*, **240**, 514.
Whitworth, A. 1979, *M.N.R.A.S.*, **186**, 59.
Wilson, O. C., Münch, G., Flather, E., and Coffeen, M. E. 1959, *Ap. J. Suppl.*, **4**, 199.
Yorke, H. W. 1986, *Ann. Rev. Astr. Ap.*, **24**, 49.
Zel'dovich, Ya. B., and Raizer, Yu. P. 1967, *Physics of Shock Waves and High-Temperature Phenomena* (New York: Academic).

PETER BODENHEIMER: Lick Observatory, University of California, Santa Cruz, CA 95064

JOSÉ FRANCO: Instituto de Astronomía-UNAM, Apdo. Postal 70-264, 04510 México D. F., México

GUILLERMO TENORIO-TAGLE: Max-Planck-Institut für Astrophysik, D-8046 Garching bei München, Federal Republic of Germany